A156 662

Radome Analysis and Design Capabilities of the RF and Microwave Technology Branch

by
P. L. Overholt
Research Department

APRIL 1985

NAVAL WEAPONS CENTER
CHINA LAKE, CA 93555-6001

DTIC
ELECTE
JUL 11 1985
S D
B

Best Available Copy

FILE COPY

Approved for public release; distribution is unlimited

Naval Weapons Center

AN ACTIVITY OF THE NAVAL MATERIAL COMMAND

FOREWORD

The research described in this report was performed at the Naval Weapons Center during fiscal years 1982 through 1984 and was supported by 6.2 Independent Exploratory Development and 6.1 Independent Research funds. This work is compiled to provide ready information for those working with radomes.

The report has been reviewed for technical accuracy by D. J. Wilcox, Code 3814, and J. D. Hall, Code 3957.

Approved by
E. B. ROYCE, Head
Research Department
9 April 1985

Under authority of
K. A. DICKERSON
Capt., USN
Commander

Released for publication by
B. W. HAYS
Technical Director

NWC Technical Publication 6636

Published by . . . . . Technical Information Department
Collation . . . . . Cover, 20 leaves
First printing . . . . . 95 copies

Best Available Copy

Best
Available
Copy

UNCLASSIFIED

SECURITY CLASSIFICATION OF THIS PAGE (When Data Entered)

REPORT DOCUMENTATION PAGE		READ INSTRUCTIONS BEFORE COMPLETING FORM
1. REPORT NUMBER NWC TP 6636	2. GOVT ACCESSION NO. AD-A156667	3. RECIPIENT'S CATALOG NUMBER
4. TITLE (and Subtitle) Radome Analysis and Design Capabilities of the RF and Microwave Technology Branch		5. TYPE OF REPORT & PERIOD COVERED Interim Report Fiscal Years 1982-1984
		6. PERFORMING ORG. REPORT NUMBER
7. AUTHOR(s) P. L. Overfelt		8. CONTRACT OR GRANT NUMBER(s)
9. PERFORMING ORGANIZATION NAME AND ADDRESS Naval Weapons Center China Lake, CA 93555-6001		10. PROGRAM ELEMENT, PROJECT, TASK AREA & WORK UNIT NUMBERS 61152N
11. CONTROLLING OFFICE NAME AND ADDRESS Naval Weapons Center China Lake, CA 93555-6001		12. REPORT DATE April 1985
		13. NUMBER OF PAGES 38
14. MONITORING AGENCY NAME & ADDRESS(if different from Controlling Office)		15. SECURITY CLASS. (of this report) UNCLASSIFIED
		15a. DECLASSIFICATION/DOWNGRADING SCHEDULE

16. DISTRIBUTION STATEMENT (of this Report)

Approved for public release; distribution is unlimited.

17. DISTRIBUTION STATEMENT (of the abstract entered in Block 20, if different from Report)

18. SUPPLEMENTARY NOTES

19. KEY WORDS (Continue on reverse side if necessary and identify by block number)

Radomes
Plane Wave Ray Tracing
Boresight Error
Reflection and Transmission Coefficients
Spherical Waves

20. ABSTRACT (Continue on reverse side if necessary and identify by block number)

See back of form.

DD FORM 1 JAN 73 1473 EDITION OF 1 NOV 65 IS OBSOLETE
S/N 0102-LF-014-6601

UNCLASSIFIED
SECURITY CLASSIFICATION OF THIS PAGE (When Data Entered)

(U) Radome Analysis and Design Capabilities of the RF and Microwave Technology Branch, by P. L. Overfelt. China Lake, Calif., Naval Weapons Center, April 1985. 38 pp. (NWC TP 6636, publication UNCLASSIFIED.)

(U) A description of computer codes covering boresight error prediction, flat panel reflection and transmission properties, Von Karman geometry parameters, and spherical wave propagation for radomes is presented. The theoretical basis for each code is discussed, and examples of inputs and outputs are given. Comparison of theory with experimental data shows reasonable correlation. Thus, these codes can predict many interesting and useful properties needed for adequate initial radome design without resorting to expensive and time-consuming test procedures.

CONTENTS

Introduction 3

Theory and Discussion 3
Boresight Error Codes 4
Flat Panel Codes 4
Von Karman Geometry Codes 5
Spherical Wave/Spherical Radome Codes 5

Inputs and Outputs 6
Boresight Error Codes 6
Flat Panel Codes 6
Spherical Wave/Spherical Radome Codes 7

Summary 7

Future Work 7

References 9

Appendixes:
A. Coordinate System for Three-Dimensional Radome 27
B. Multilayer Isotropic Flat Panel Equations 31
C. Multilayer Uniaxially Anisotropic Flat Panel Equations . . 35
D. Von Karman Geometry 37

DTIC COPY INSPECTED

Accession For
NTIS GRA&I ☑
DTIC TAB ☐
Unannounced ☐
Justification
By
Distribution/
Availability Codes
Dist | Avail and/or Special
A-1

INTRODUCTION

Several years ago the Naval Weapons Center (NWC) embarked on an effort to establish expertise in the areas of radome analysis, design, and testing. An interdepartmental program was devised to develop structural, thermal, and electromagnetic capabilities at NWC and to upgrade existing test facilities. As a result of this program, the RF and Microwave Technology Branch, Code 3814, has become knowledgeable in the area of electromagnetic radome analysis and has created a number of computer codes which can predict many useful properties of radomes. Starting with the simplest of models and progressing toward more complex variations, we have built up a large library of subroutines which can be combined in various ways to give a very flexible radome analysis capability.

This report contains a description of the general theory for analyzing radomes. The various types of computer codes are described in the section on Theory and Discussion. Examples of the inputs and outputs of each code are presented in the section which carries that title. The Summary discusses all progress to date, and the expectation of work to be done is detailed under Future Work.

At the time of this writing, our electromagnetic analysis effort will continue for at least one more year. Thus, all work is ongoing and subject to change.

THEORY AND DISCUSSION

The electromagnetic radome codes can be divided into four general groups. Each code in a group is completely self-sufficient, yet is related to the codes in all other groups. The first group predicts boresight error as a function of antenna gimbal angle. The second group computes reflection and transmission coefficients for a multilayer system of flat (no curvature) surfaces. The third group computes various parameters characterizing two-dimensional Von Karman shaped radomes, and the fourth group consists of codes based on the propagation of spherical waves through spherical radomes.

BORESIGHT ERROR CODES

The boresight error codes calculate boresight error as a function of antenna gimbal (look) angle using the technique of plane wave ray tracing. There are three codes in this group: (1) two-dimensional boresight error transmit formulation; (2) two-dimensional boresight error receive formulation using monopulse processing; and (3) three-dimensional boresight error receive formulation, also using monopulse processing.

The transmit case is based on the following theory. An antenna is placed inside the radome and divided into equidistant point sources (Figure 1), each of which emits a ray traveling perpendicular to the antenna. The points at which each ray intersects the radome are computed, the normals at these points are found, and the incidence angles at which each ray strikes the radome are calculated. The flat panel transmission and reflection coefficients are used for multiple isotropic layers, and the rays are refracted as they propagate through varying dielectric constants, which differ from that of free space. The rays are then extended to a constant phase plane outside the radome where a best-fit, least-squares technique is used to form a straight line through the points in this phase plane. The difference between the tilt angle of this line and the gimbal angle of the antenna is the boresight error.

The receive formulations (both two- and three-dimensional) are very similar except that an infinite plane wave is assumed incident from outside the radome (see Figure 2) and is divided into equidistant points. Each point emits a ray traveling perpendicular to the incident plane wave which intersects the radome. As in the transmit formulation, the intersection points, normals to the radome at those points, incidence angles, and transmission and reflection coefficients are computed. The rays are then extended to the antenna which is divided in half for two dimensional and in quadrants for three dimensional. The received signal amplitude is computed over each half-quadrant of the antenna, and the monopulse equations are used to compute the boresight error. The two-dimensional formulation provides only principal plane boresight error prediction, while the three-dimensional receive formulation in Figure 3 provides information for all planes (see Appendix A).

FLAT PANEL CODES

Because the flat panel transmission and reflection properties for multiple-layer radomes are such an important part of the previous boresight error codes, we have created two programs which calculate these cumulative complex transmission and reflection coefficients as functions of frequency with incidence angle as a parameter. One code

assumes that all layers are isotropic (see Figure 4), while the second assumes that all layers are uniaxially anisotropic (Reference 1), i.e., the dielectric constant along the axis normal to the surface is different from that in the plane of the surface (see Figure 5). Both codes first calculate the single-surface reflection coefficients for both parallel and perpendicular polarizations. Then the flat-panel coefficients for each layer are computed (Reference 2). The layers are then cascaded using signal flow graph theory to provide the overall complex transmission and reflection coefficients for multiple layers (see Appendixes B and C).

VON KARMAN GEOMETRY CODES

The majority of our electromagnetic analysis to date has concentrated on Von Karman shaped radomes, although the codes are set up in such a way that extensions to any desired shape are easily implemented. As a result, there are two codes which calculate various values characterizing a two-dimensional Von Karman radome. One computes the functional value, first derivative or slope, second derivative, and radius of curvature as functions of position along the radome (see Appendix D). The other computes the radome radius and the clearance of an antenna that is gimballed inside the radome at any point along the axis. This code can handle not only a constant wall thickness between the inner and outer shapes but also a linearly tapered wall.

SPHERICAL WAVE/SPHERICAL RADOME CODES

Finally, in our efforts to progress toward more complex, physically satisfying models, we have developed two programs based on propagation of spherical waves from a dipole antenna. One uses an approximate spherical wave ray tracing method (Reference 3) and calculates the electric field magnitude as a function of polar angle for a dipole offset along the axis of a spherical radome. The second code calculates exactly the same quantities but uses the boundary-value method to compute the exact solution (Reference 4). These two solutions are then compared to show those conditions which limit the accuracy of the spherical wave ray tracing approach (Reference 5). While these two codes are applicable only to spherical radomes, their comparison has produced insights into the limitations of spherical wave ray tracing which can be applied to other more typical radome shapes.

INPUTS AND OUTPUTS

BORESIGHT ERROR CODES

The two-dimensional boresight error codes require inputs specifying the radome shape, material parameters characterizing the various layers, antenna size and frequency, and polarization information. Specifically, the user must input frequency, length, and diameter of the Von Karman shape, antenna position along the radome axis, antenna diameter, dielectric constant, loss tangent and thickness for each layer, total number of layers, number of points into which the antenna length is divided, and parallel or perpendicular polarization. The three-dimensional code requires all of the above inputs with roll angle, antenna polarization, and incident plane wave polarization as additional parameters.

Examples of the output of these three codes are given in Figures 6 through 8, while comparison with recent experimental data taken in our radome test chamber is shown in Figure 9. Reasonable correlation between theory and experiment at X-band frequencies has been achieved using the plane wave ray tracing approach, although certain discrepancies have been found at lower frequencies. These discrepancies are being investigated currently. Figures 10 and 11 are outputs from the boresight error transmit formulation code. Average and central ray transmission magnitudes versus gimbal angle are plotted from a modified version.

FLAT PANEL CODES

The flat panel codes which plot reflection and transmission versus frequency require inputs consisting of minimum and maximum frequency values, a frequency increment, angle of incidence (in degrees), number of layers, and dielectric constants, loss tangents, and thicknesses of each layer.

Examples of the output of the isotropic code are given in Figures 12 through 14.* These codes provide an exact (no approximations) analysis of any multilayer isotropic or uniaxially anisotropic flat panel system.

*Examples of outputs from the uniaxially anisotropic flat panel code are not included since they would look virtually identical except for dielectric constant.

SPHERICAL WAVE/SPHERICAL RADOME CODES

Inputs to the spherical radome programs are inner and outer radii, dipole offset distance, wavelength, index of refraction (real only), and observation radius. These codes plot the electric field magnitude as found by both the ray tracing method and the exact method as a function of the polar angle θ. Comparison of the two techniques is shown in Figure 15, assuming increasing source offset distance. Comparison of the exact theory with experiment is shown in Figure 16 (Reference 4).

SUMMARY

An overview describing computer codes for electromagnetic analysis and design of radomes has been presented. These codes provide a broad base for predicting the electromagnetic properties of radomes without requiring costly and time-consuming testing procedures. As such they serve as an efficient design tool for establishing an initial baseline radome configuration. We have created nine different codes which compute boresight error, reflection and transmission properties based on flat panel models, Von Karman geometry characteristics, and spherical wave propagation effects. Plane wave ray tracing has been the standard approximation technique upon which the boresight error codes are based. The remaining codes, except for the spherical wave ray tracing code, are all exact solutions which can be used in many different types of problems. We have tried to develop a versatile and flexible radome analysis capability which can be used in practical applications.

FUTURE WORK

Many relatively small modifications are planned in the next phase of the radome analysis and design program. We will modify the boresight error codes to include weighting functions which reflect different antenna aperture distributions. Both amplitude and phase weighting will be considered. Different radome shapes, curvature, multiple reflections (ghost lobes), complex permeabilities, tapered radomes, and nonconstant wall thicknesses will be included eventually in the boresight error codes. Elliptical polarization will be built into the flat panel codes. The effects of tuning or taping a radome to reduce its boresight error will be analyzed.

Several discrepancies among the boresight error codes have been discovered at frequencies below X-band, i.e., 2 to 8 gigahertz. We are currently examining our monopulse processing methods and deriving more

rigorous equations for this aspect of the two- and three-dimensional receive formulations which should correct this problem.

Finally, the spherical wave/spherical radome codes will be modified to include multilayers, and we will use the spherical wave ray tracing code as a starting point for our own more rigorous Huyghen's principle spherical wave ray tracing method (see Figure 17).

REFERENCES

1. D. J. White and D. J. Banks. "Plane Wave Transmission and Reflection Coefficients for Anisotropic Sheets of Radome Material," in Proceedings of the 16th Symposium on Electromagnetic Windows. Georgia Institute of Technology, Atlanta, June 1982. Pp. 7-12.

2. Air Force Weapons Laboratory. Techniques for Airborne Radome Design, Vol. I, by T. E. Tice. Albuquerque, N.M., December 1966, Chapter 2. (Technical Report AFAL-TR-66-391, publication UNCLASSIFIED.)

3. S. W. Lee, M. S. Sheshadri, V. Jamnejaid, and R. Mittra. "Wave Transmission Through a Spherical Dielectric Shell," IEEE Trans. Antennas Propag., Vol. AP-30, No. 3 (May 1982), pp. 373-80.

4. C. T. Tai and R. I. Barnett. "Characteristics of Large Spherical Radomes," in Proceedings of O.S.U.-W.A.D.C Radome Symposium, Vol. I. Antenna Laboratory, Ohio State University, Columbus, June 1955. Pp. 77-93.

5. D. A. Bloom, P. L. Overfelt, and D. J. White. "Comparison of Spherical Wave Ray Tracing and Exact Boundary Value Solutions for Spherical Radomes," in Proceedings of the 17th Symposium on Electromagnetic Windows. Georgia Institute of Technology, Atlanta, July 1984. Pp. 17-21.

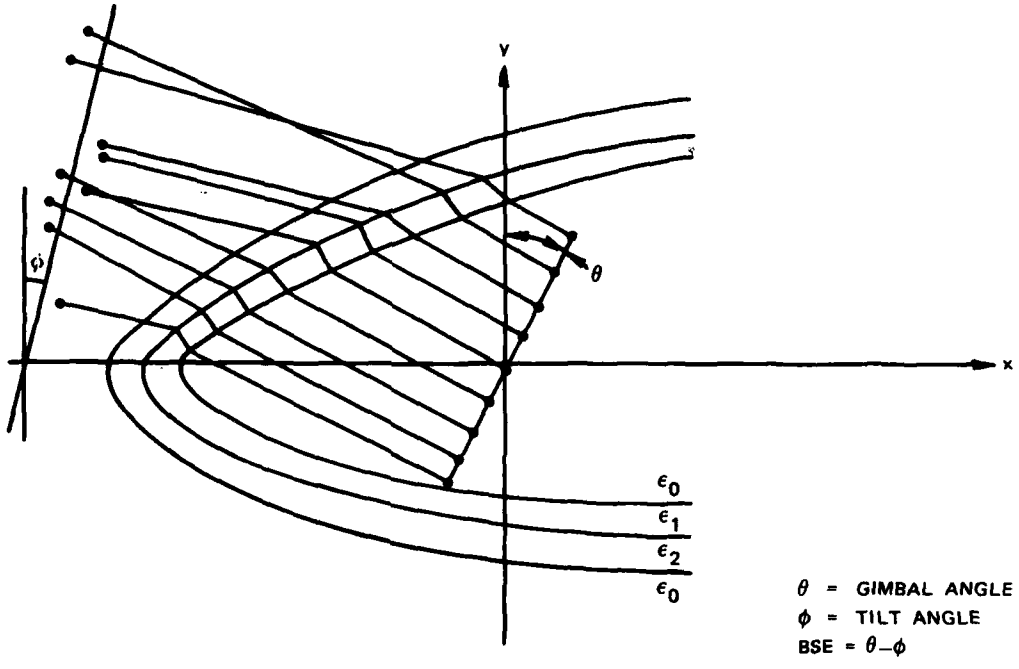

FIGURE 1. Two-Dimensional Boresight Error Transmit Formulation.

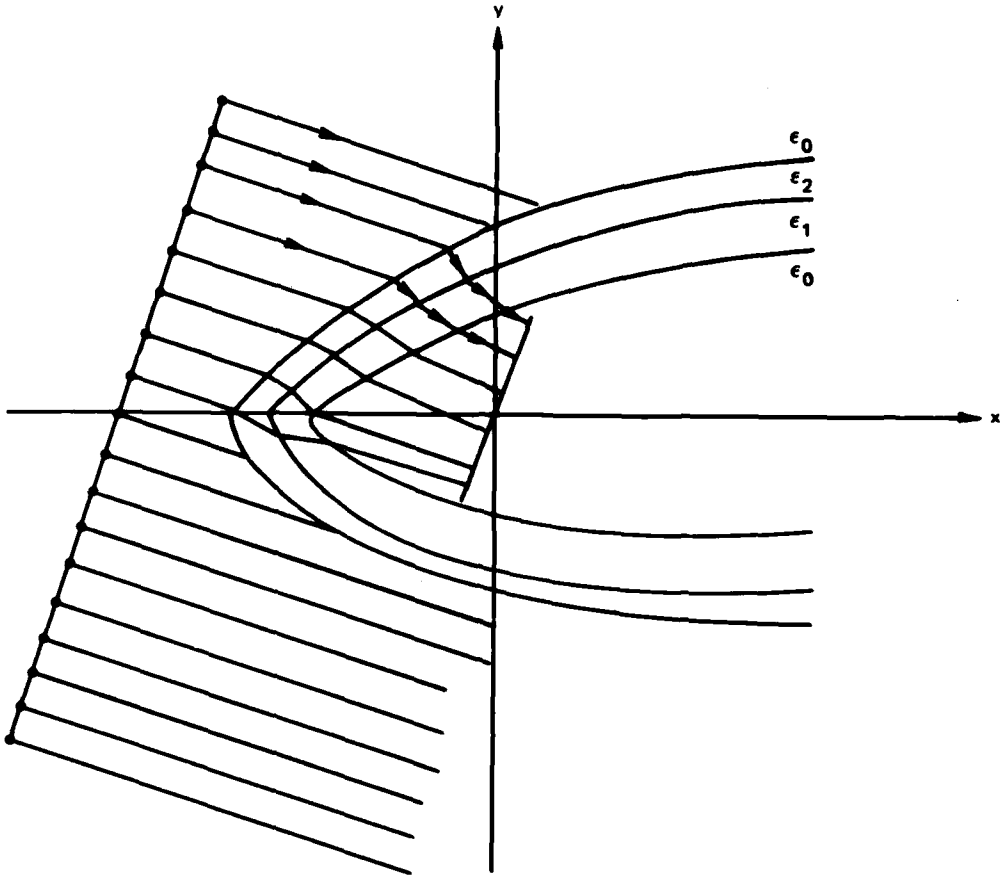

FIGURE 2. Two-Dimensional Boresight Error Receive Formulation.

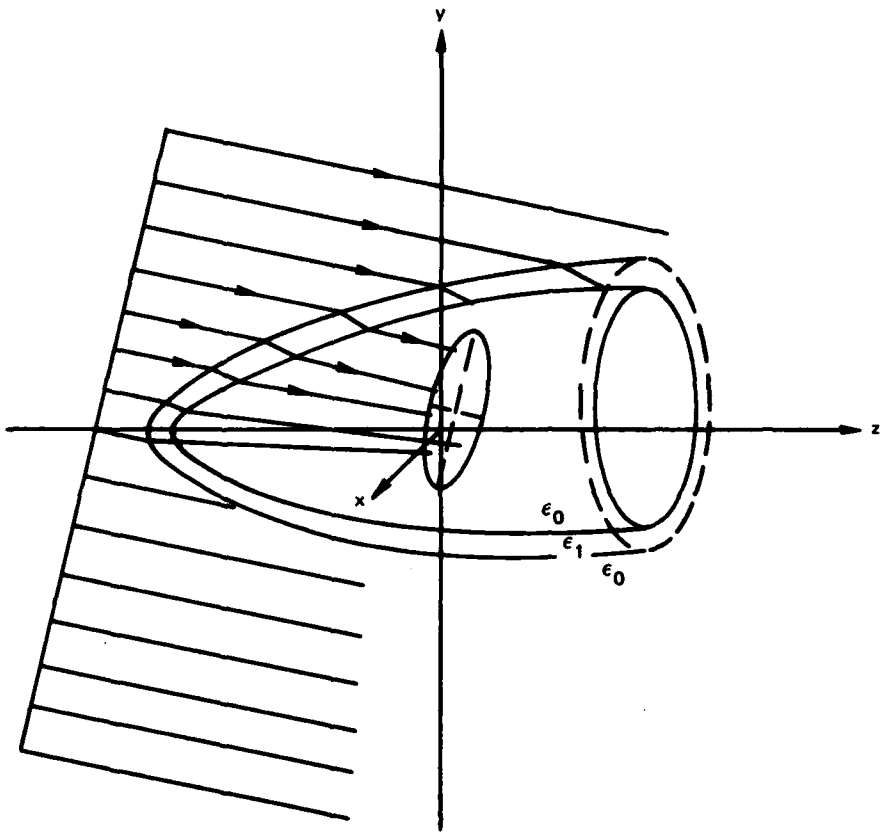

FIGURE 3. Three-Dimensional Boresight Error Receive Formulation.

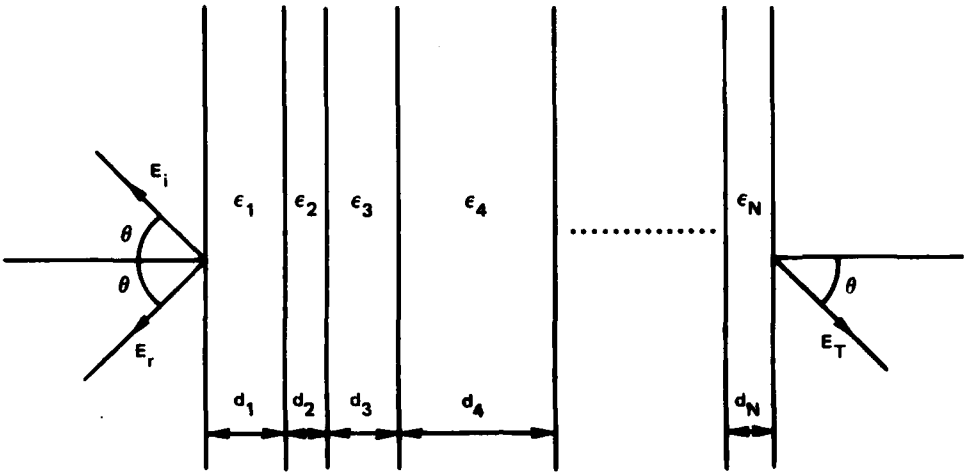

FIGURE 4. Multilayer Isotropic Flat Panel System.

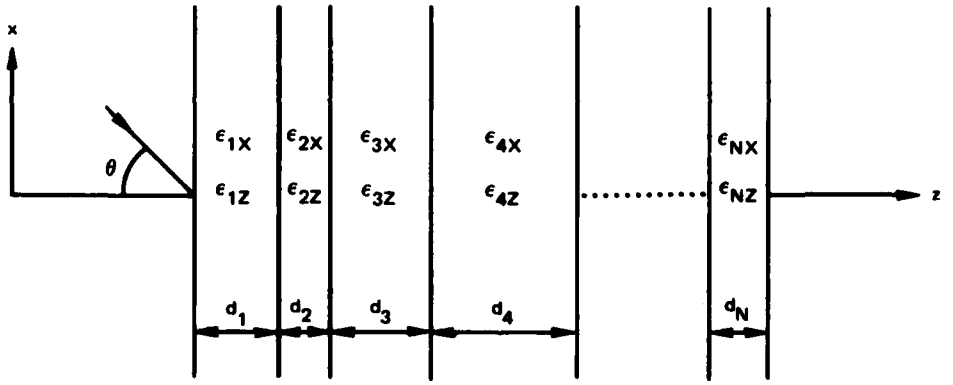

FIGURE 5. Multilayer Uniaxially Anisotropic Flat Panel System.

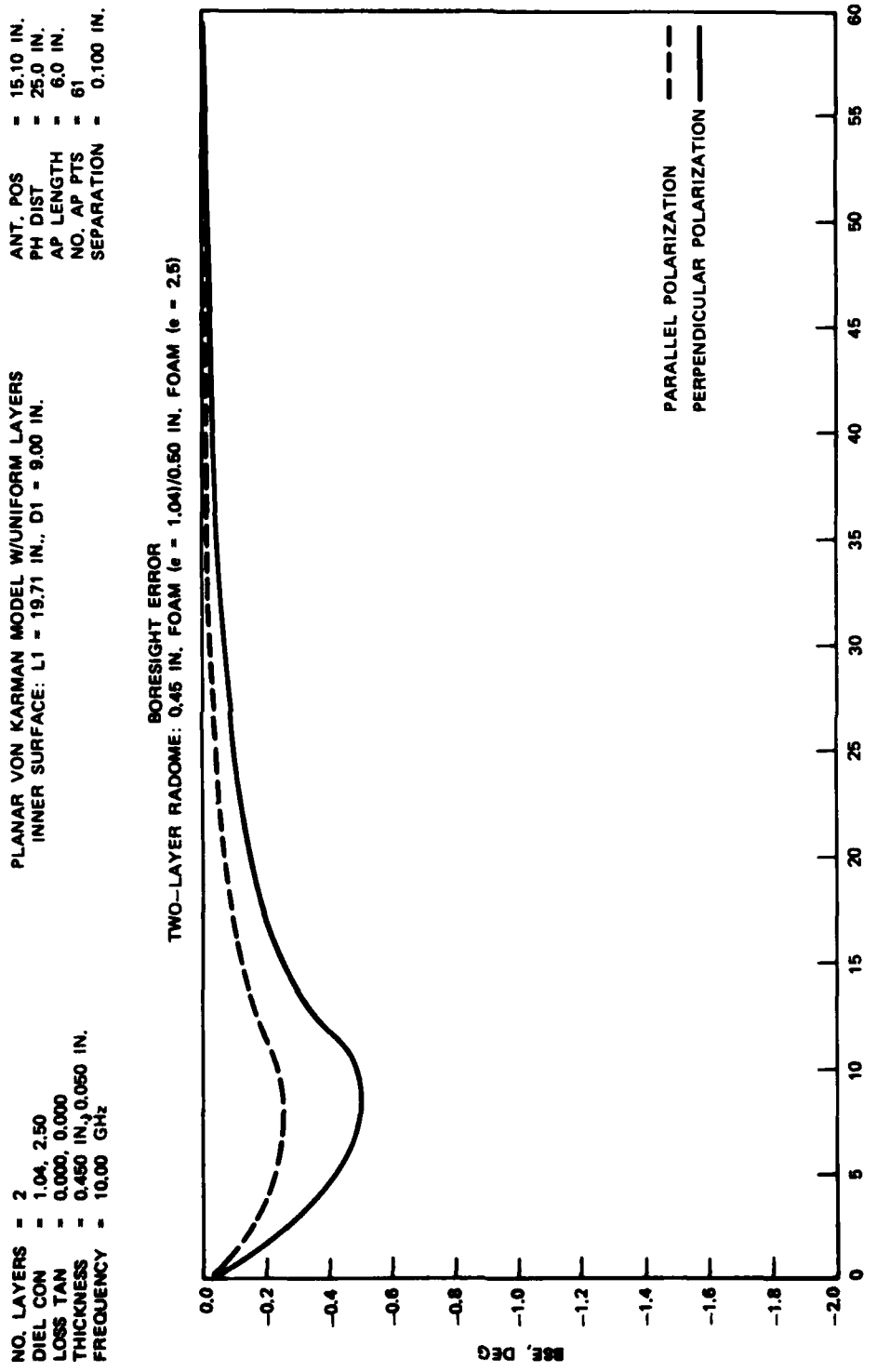

FIGURE 6. Boresight Error from Two-Dimensional Transmit Formulation.

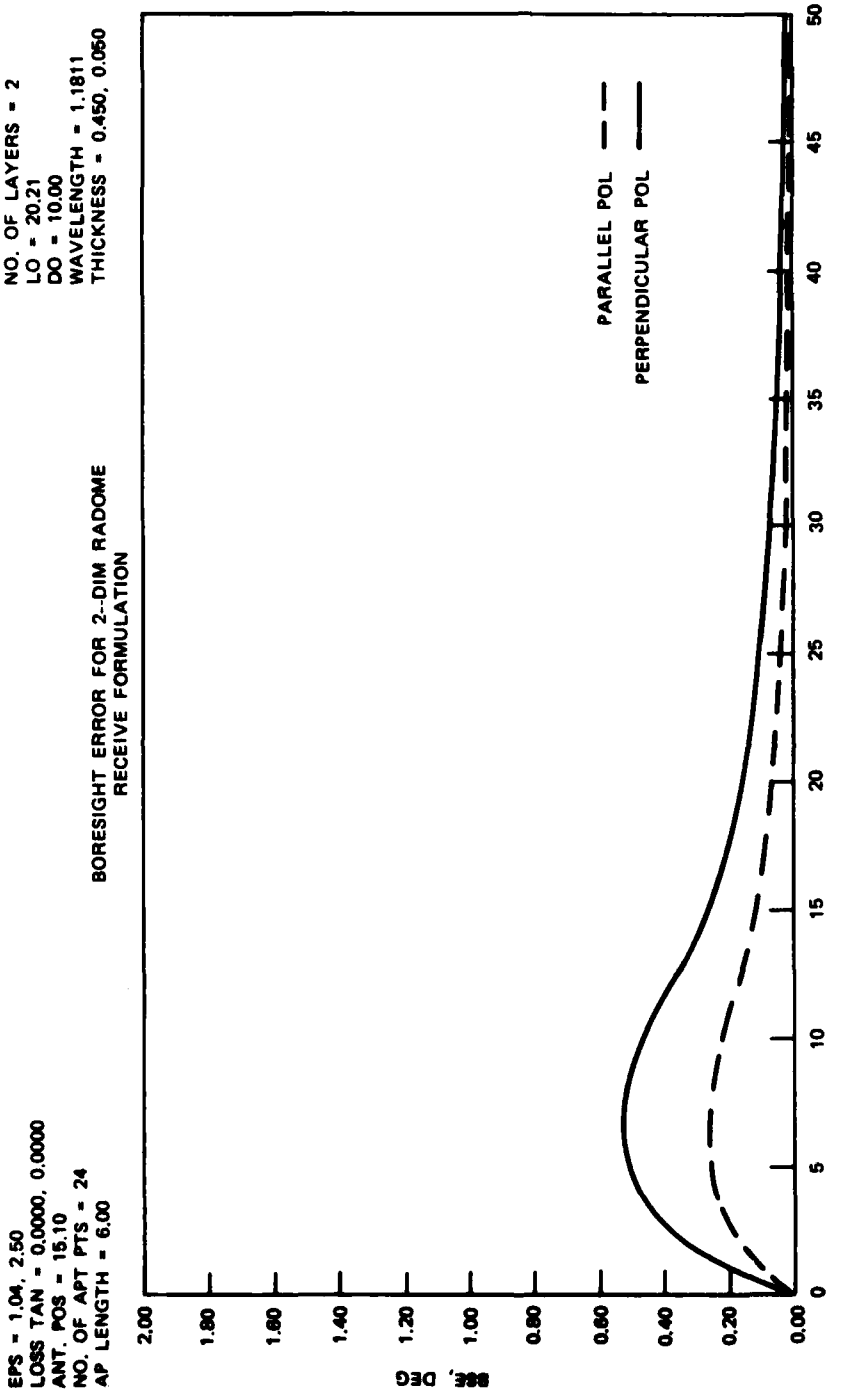

FIGURE 7. Boresight Error from Two-Dimensional Receive Formulation.

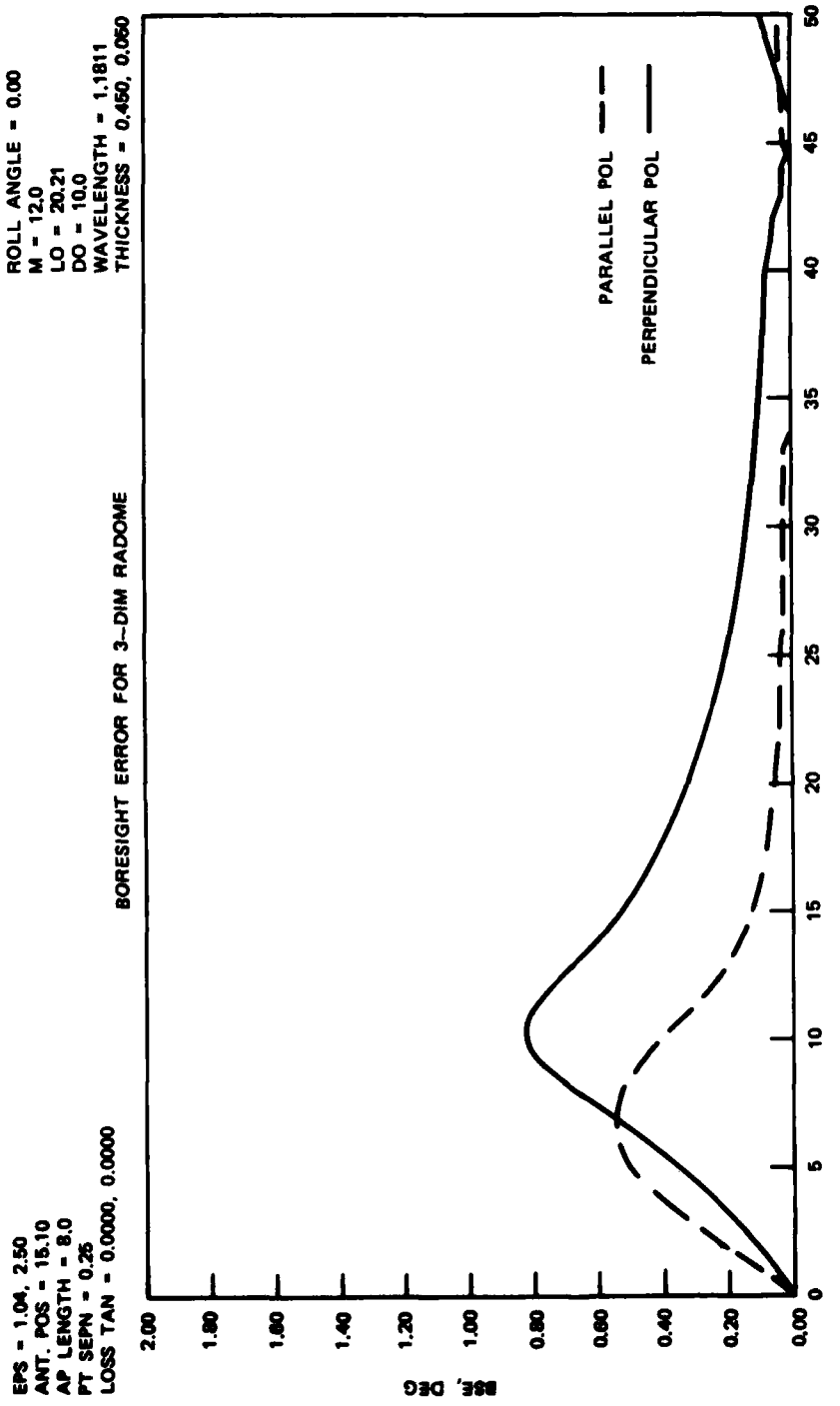

FIGURE 8. Boresight Error from Three-Dimensional Receive Formulation.

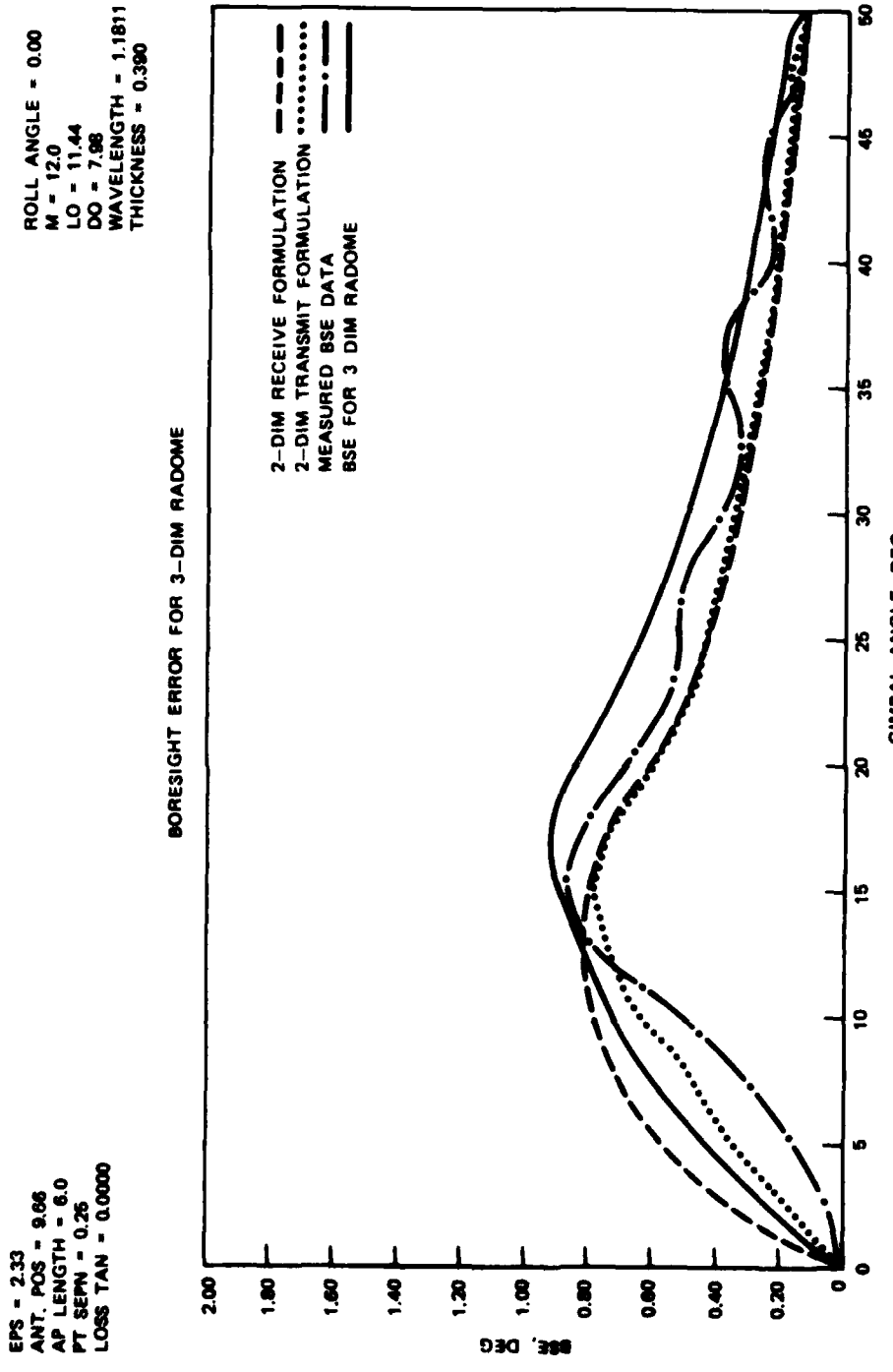

FIGURE 9. Comparison of Three Boresight Error Formulations with Experimental Data.

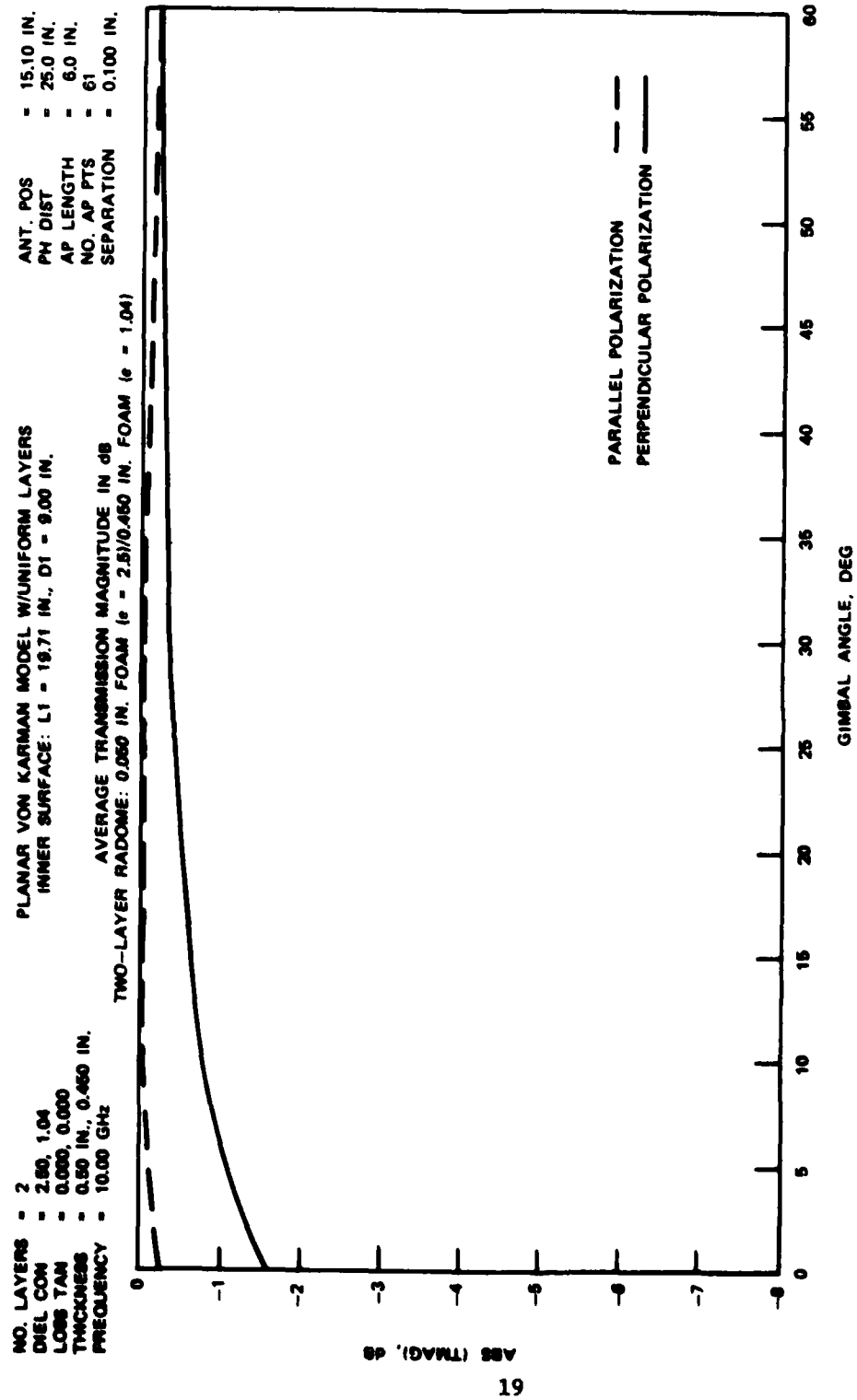

FIGURE 10. Average Transmission Magnitude from Two-Dimensional Transmit Formulation.

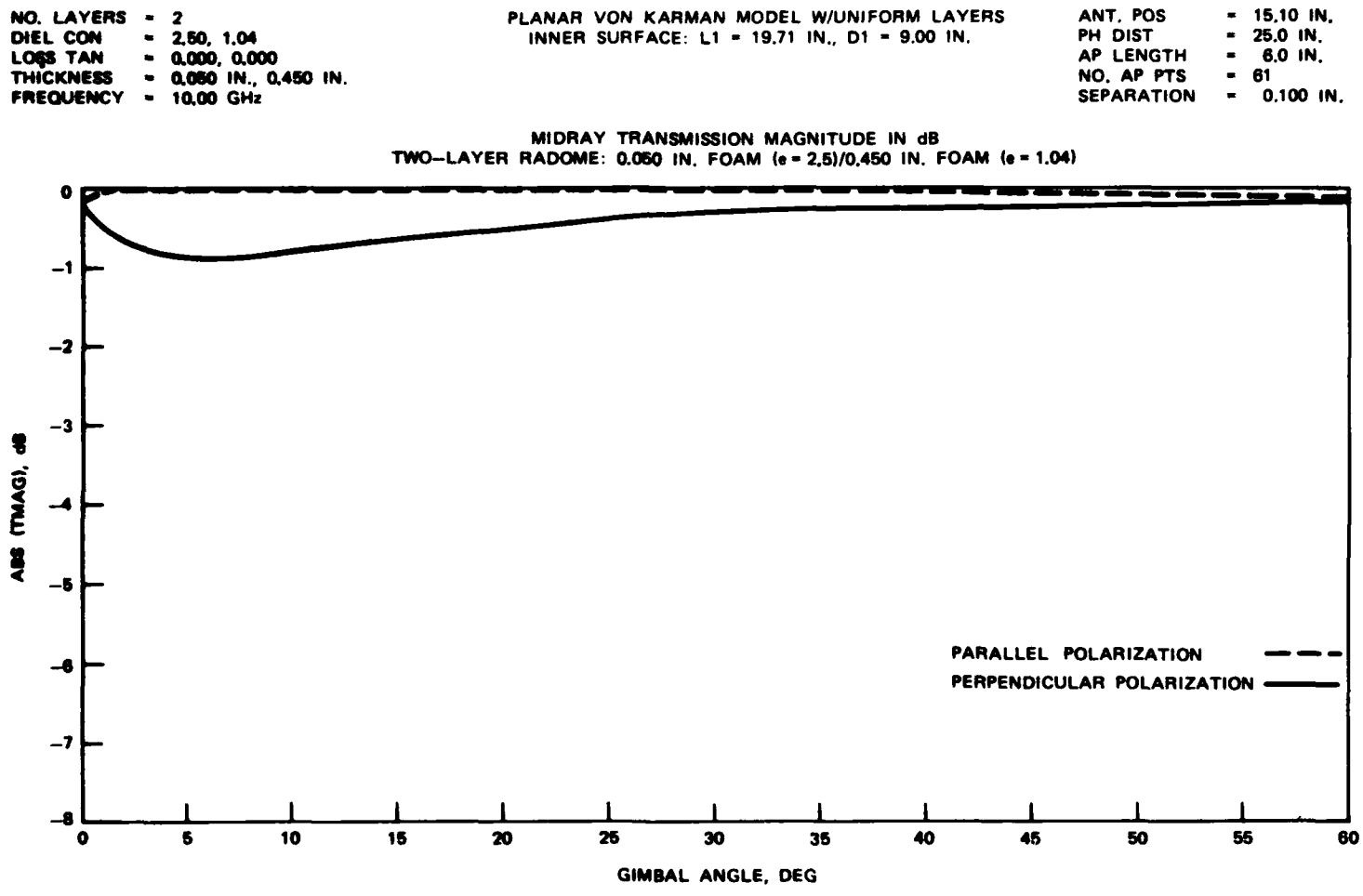

FIGURE 11. Midray Transmission Magnitude from Two-Dimensional Transmit Formulation.

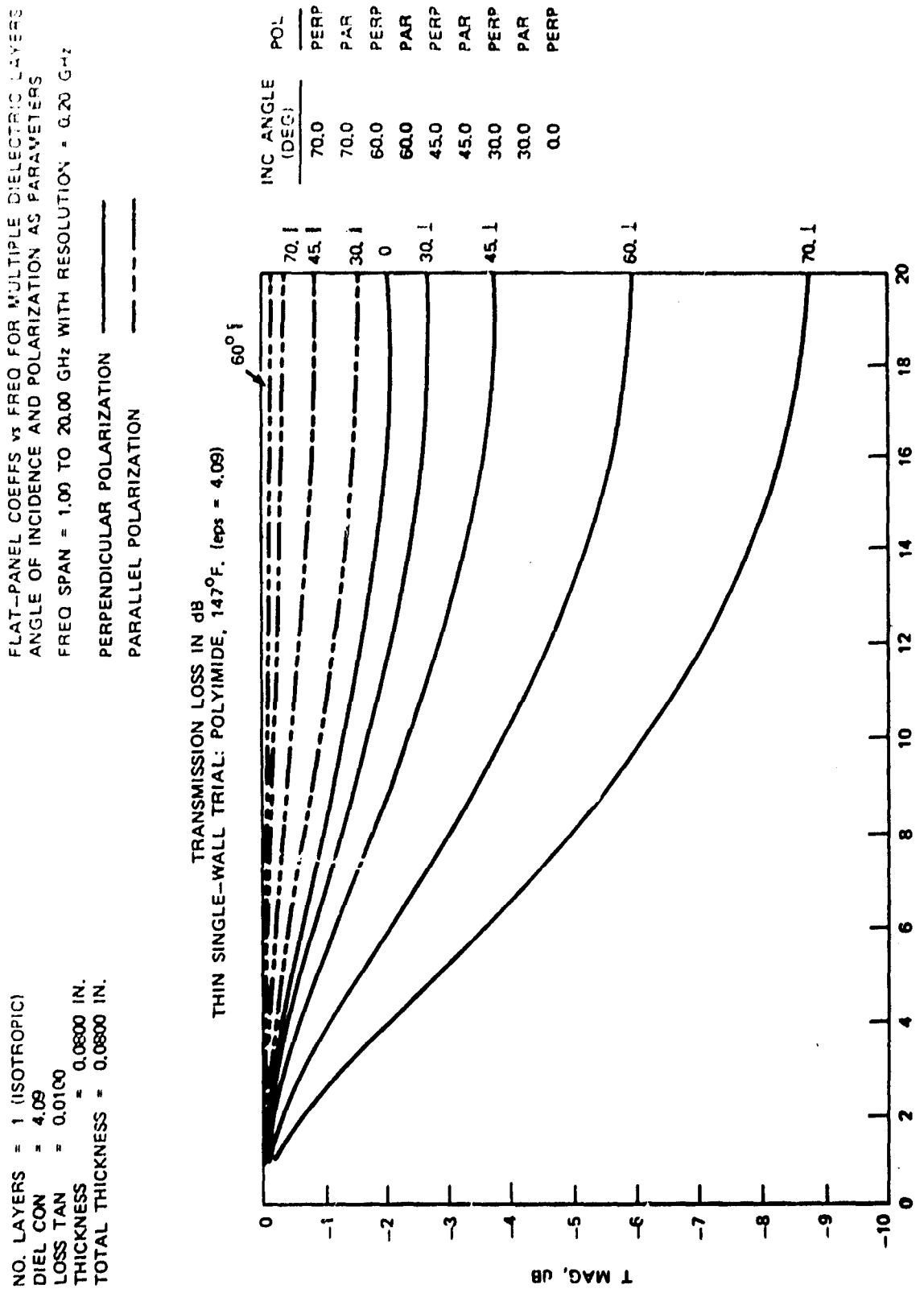

FIGURE 12. Transmission Loss Versus Frequency.

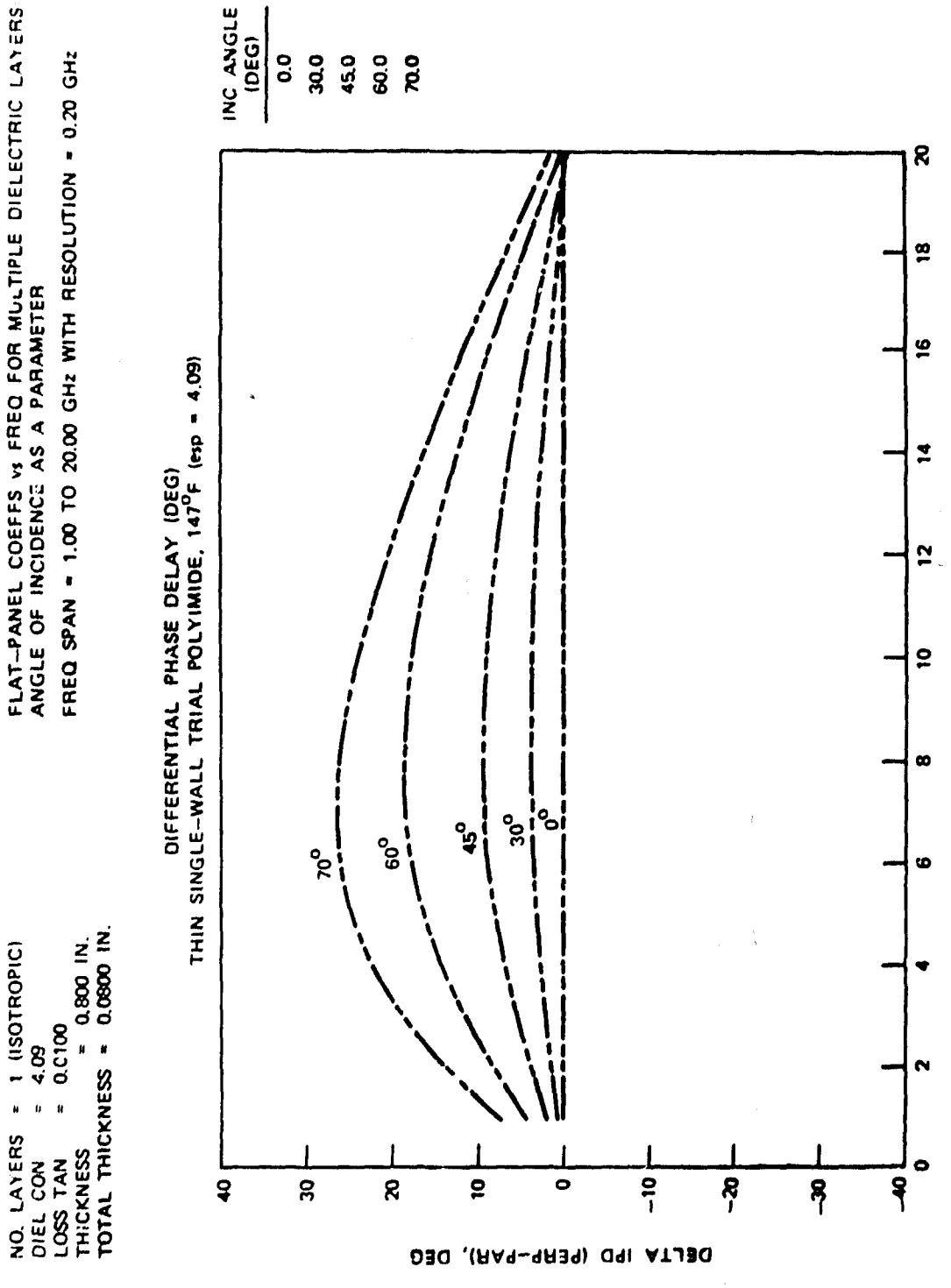

FIGURE 13. Differential Phase Delay Versus Frequency.

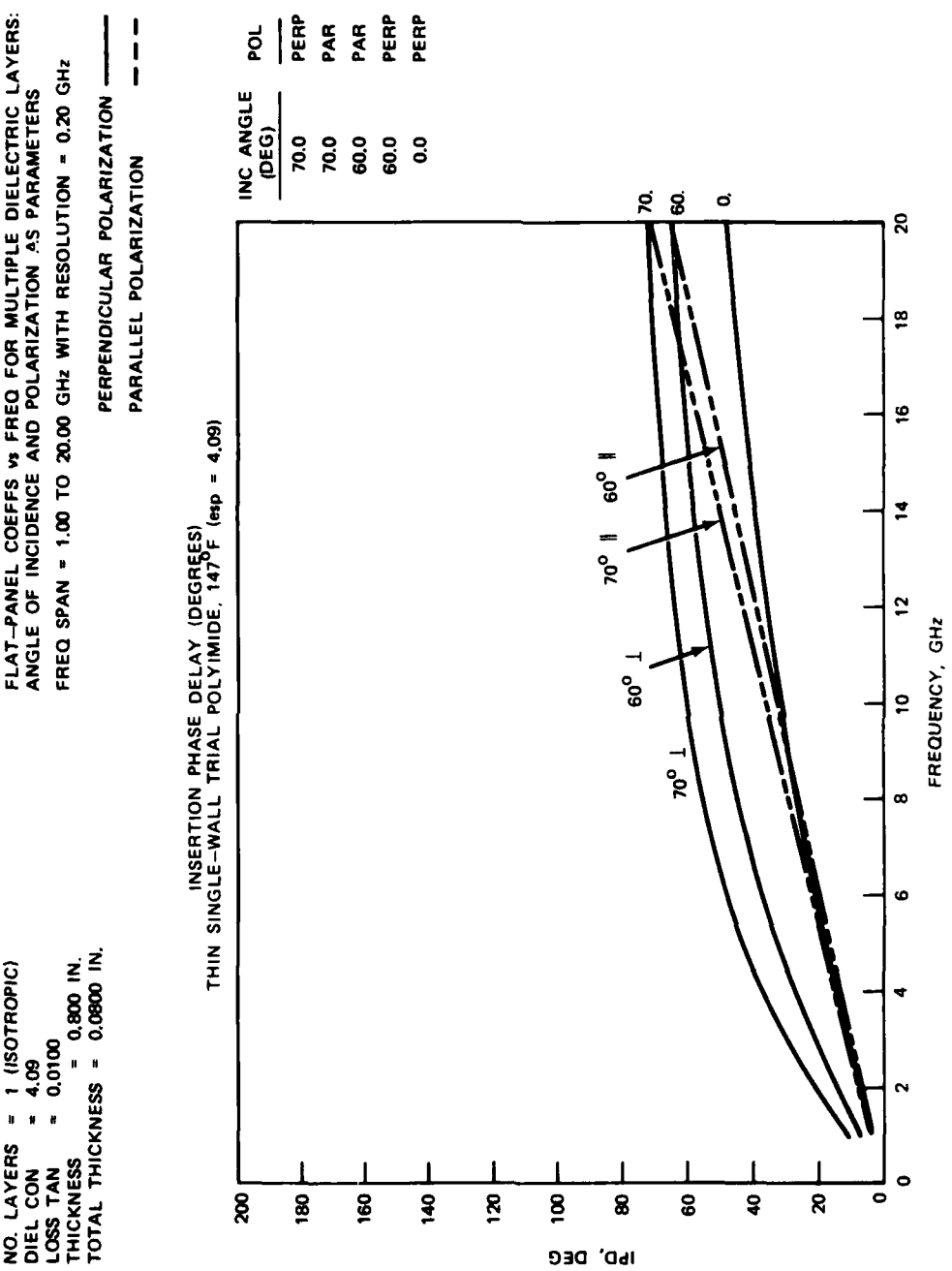

FIGURE 14. Insertion Phase Delay Versus Frequency.

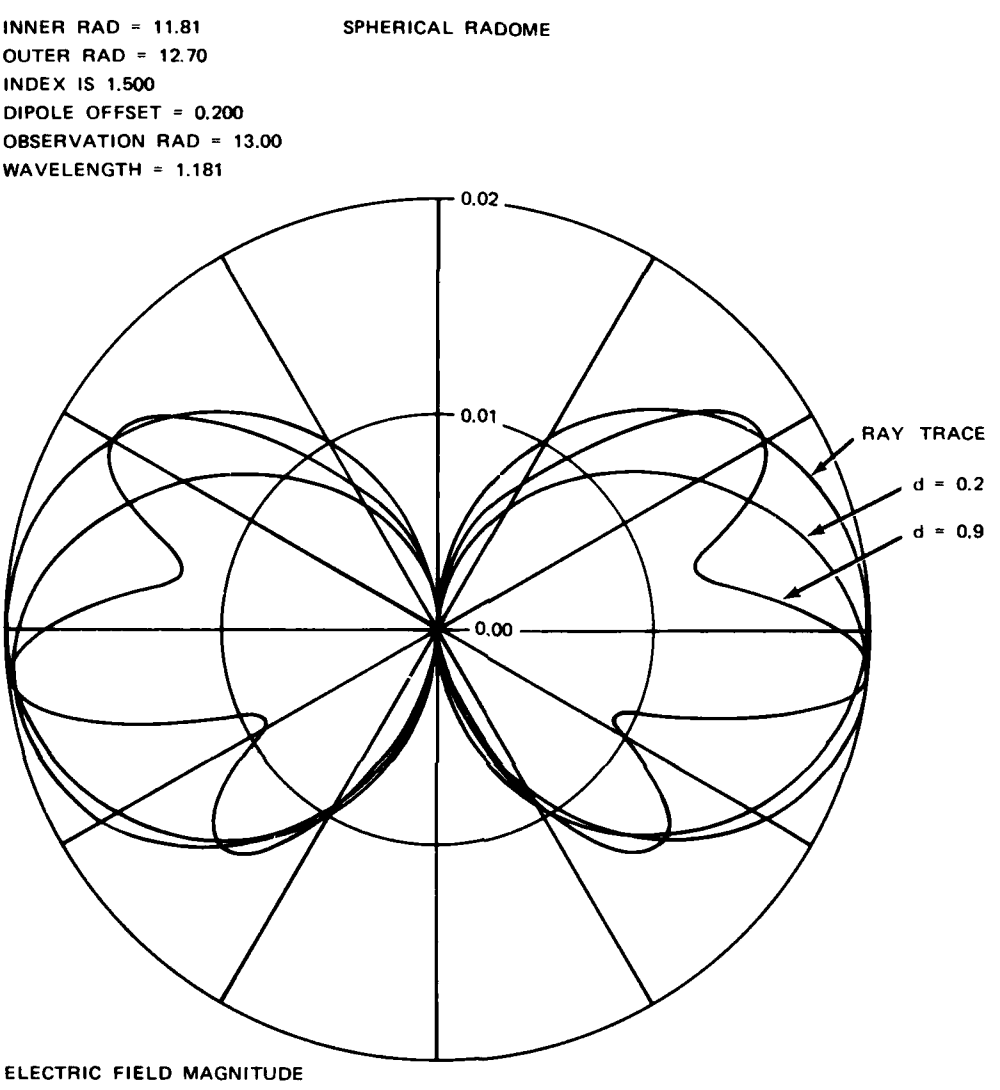

FIGURE 15. Effect of Increasing Dipole Offset Distance.

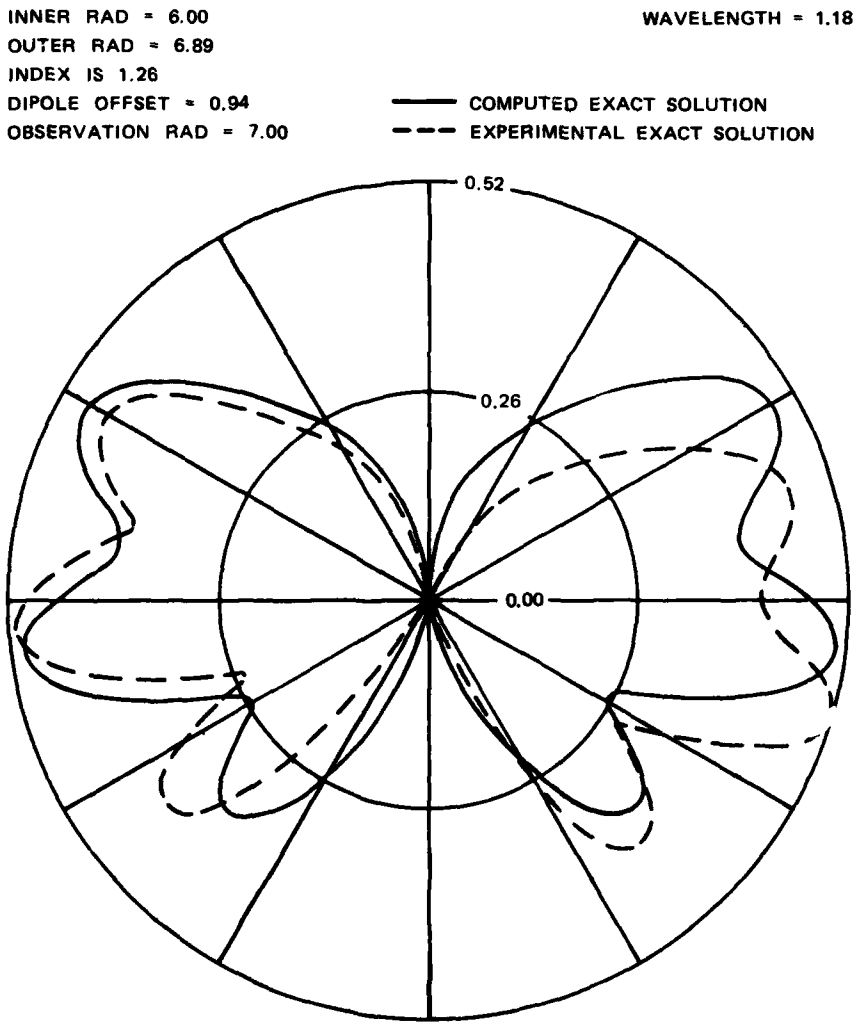

FIGURE 16. Comparison of Experimental and Computed Exact Solutions.

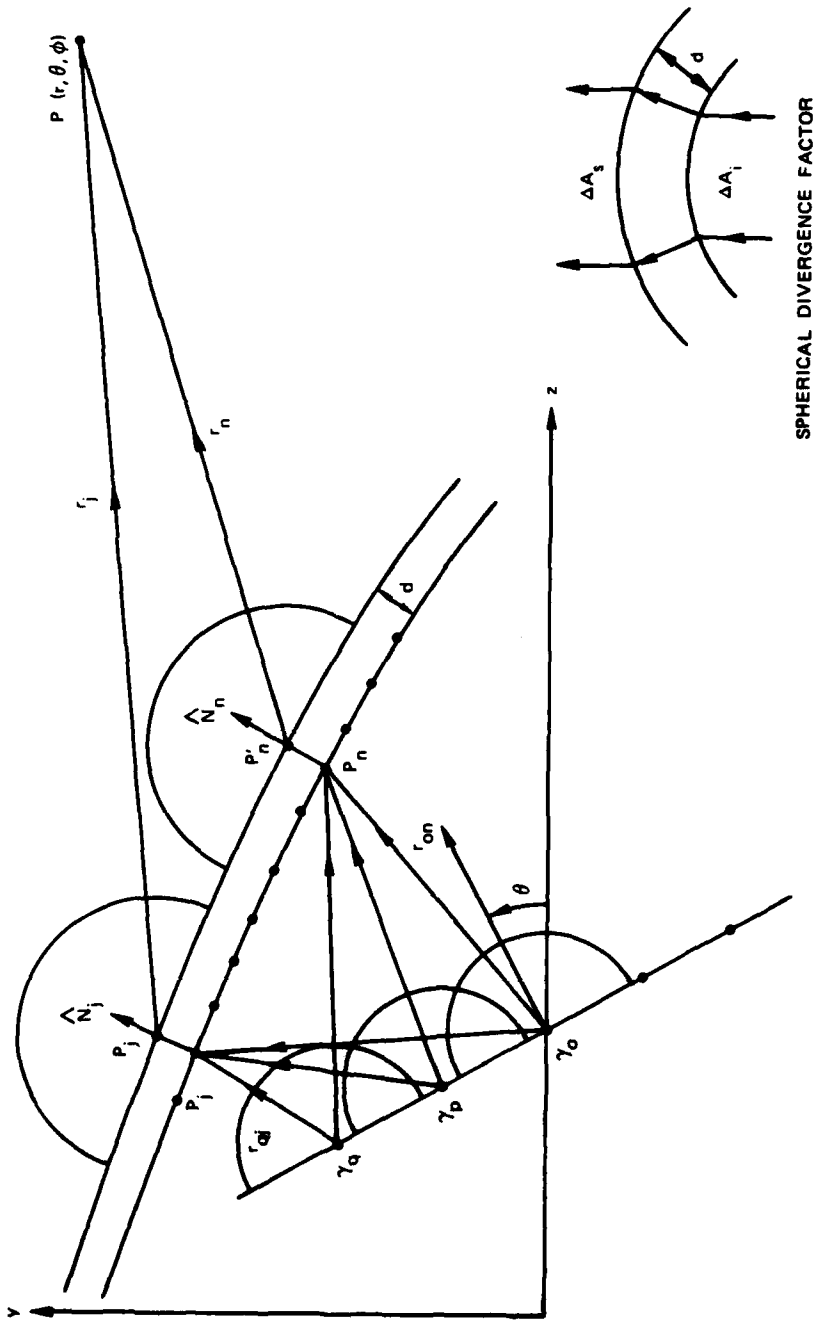

FIGURE 17. Huyghen's Principle Spherical Wave Ray Tracing Method.

Appendix A

COORDINATE SYSTEM FOR THREE-DIMENSIONAL RADOME

In radome coordinates, we have

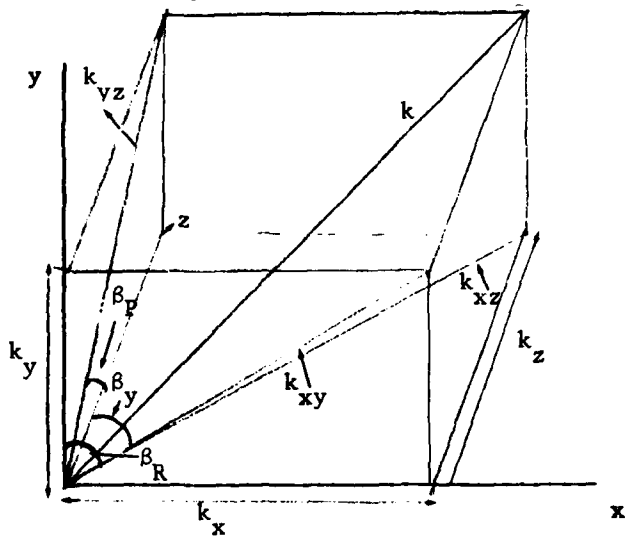

k = propagation vector

k_{xy} = projection of k in the xy plane

k_{xz} = projection of k in the xz plane

k_{yz} = projection of k in the yz plane

β_R = roll angle from y-axis to k_{xy}

β_y = yaw angle from k_{xz} to z-axis

β_p = pitch angle from k_{yz} to z-axis.

Using direction cosines,

$$\hat{k} = \cos\alpha\,\hat{x} + \cos\beta\,\hat{y} + \cos\gamma\,\hat{z} \qquad \text{(A-1)}$$

where γ, the look angle, and β_R, the roll angle, are given, the relationships between direction cosines and pitch, roll, and yaw angles are given by

$$\cos\alpha = k_x = k_{xz}\sin\beta_y = \sin\beta\sin\beta_y \tag{A-2a}$$

or

$$\cos\alpha = k_{xy}\sin\beta_R = \sin\gamma\sin\beta_R \tag{A-2b}$$

$$\cos\beta = k_y = k_{xy}\cos\beta_R = \sin\gamma\cos\beta_R \tag{A-2c}$$

or

$$\cos\beta = k_{yz}\sin\beta_P = \sin\alpha\sin\beta_P \tag{A-2d}$$

$$\cos\gamma = k_z = k_{xz}\cos\beta_y = \sin\beta\cos\beta_y \tag{A-2e}$$

or

$$\cos\gamma = k_{yz}\cos\beta_P = \sin\alpha\cos\beta_P \tag{A-2f}$$

Thus, solving for the pitch, roll, and yaw angles in terms of direction cosines, we have

$$\beta_y = \tan^{-1}(\cos\alpha/\cos\gamma) \tag{A-3a}$$

$$\beta_R = \tan^{-1}(\cos\alpha/\cos\beta) \tag{A-3b}$$

$$\beta_P = \tan^{-1}(\cos\beta/\cos\gamma) \tag{A-3c}$$

Alternatively, we could write

$$\cos\alpha = [\cot^2\beta_R + \cot^2\beta_y + 1]^{-1/2} \tag{A-4a}$$

$$\cos\beta = [\tan^2\beta_R + \cot^2\beta_p + 1]^{-1/2} \tag{A-4b}$$

$$\cos\gamma = [\tan^2\beta_y + \tan^2\beta_p + 1]^{-1/2} \tag{A-4c}$$

The matrix which transforms coordinates from the antenna (double-primed) system to the radome (unprimed) system is given by*

$$\bar{x} = \begin{bmatrix} \cos\beta_y & -\sin\beta_y\cos\beta & \sin\beta_y\sin\beta \\ 0 & \sin\beta & \cos\beta \\ -\sin\beta_y & -\cos\beta_y\cos\beta & \cos\beta_y\sin\beta \end{bmatrix} \bar{x}'' \tag{A-5}$$

*We have assumed a two-axis gimbal system where Equation A-5 is derived by rotating about the original Y-axis followed by a rotation about the new X-axis.

Appendix B

MULTILAYER ISOTROPIC FLAT PANEL EQUATIONS

Using Figure 4 which shows θ as the angle of incidence for a plane wave striking a plane sheet of material composed of different dielectrics of different thicknesses,

$$r_i = \frac{\cos\theta - \sqrt{\varepsilon_i(1-j\ \tan\delta_i) - \sin^2\theta}}{\cos\theta + \sqrt{\varepsilon_i(1-j\ \tan\delta_i) - \sin^2\theta}} \quad \text{perpendicular polarization} \tag{B-1}$$

$$= \frac{\varepsilon_i(1-j\ \tan\delta_i)\cos\theta - \sqrt{\varepsilon_i(1-j\ \tan\delta_i) - \sin^2\theta}}{\varepsilon_i(1-j\ \tan\delta_i)\cos\theta + \sqrt{\varepsilon_i(1-j\ \tan\delta_i) - \sin^2\theta}} \tag{B-2}$$

parallel polarization , $i = 1,2,3...N$

The r_i (for both polarizations) are called the single-surface reflection coefficients or, alternatively, the Fresnel formulas. These form the reflection and transmission coefficients for a single layer, i.e.,

$$T_i = \frac{(1 - r_i^2)e^{-j\beta_i d_i}}{1 - r_i^2 e^{-j2\beta_i d_i}} \tag{B-3}$$

$$R_i = \frac{r_i(1 - e^{-j2\beta_i d_i})}{1 - r_i^2 e^{-j2\beta_i d_i}} \tag{B-4}$$

where

$$\beta_i = \frac{2\pi}{\lambda_o} \sqrt{\epsilon_i(1-j\ \tan\delta_i) - \sin^2\theta} \tag{B-5}$$

and λ_o is the free-space wavelength.

For a single layer, these coefficients can be cascaded using signal flow graph theory to form overall reflection and transmission coefficients for many layers.

For two layers, we have

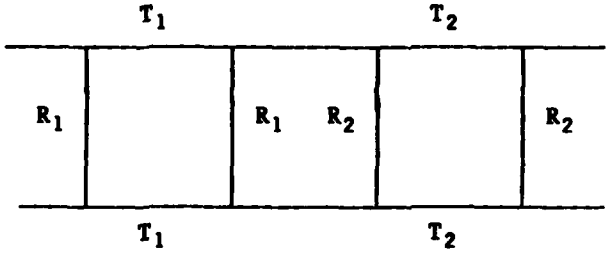

as the signal flow graph representation which can be rewritten as

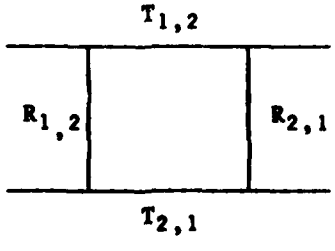

and the overall coefficients are

$$T_{1,2} = T_{2,1} = \frac{T_1 T_2}{1 - R_1 R_2} \tag{B-6}$$

$$R_{1,2} = R_1 + \frac{T_1^2 R_2}{1 - R_1 R_2} \tag{B-7}$$

$$R_{2,1} = R_2 + \frac{T_2^2 R_1}{1 - R_1 R_2} \tag{B-8}$$

Similarly, for N layers we have

$$T_{1,N} = T_{N,1} = \frac{T_{1,N-1} T_N}{1 - R_{N-1,1} R_N} \tag{B-9}$$

$$R_{N,1} = R_N + \frac{T_N^2 R_{N-1,1}}{1 - R_{N-1,1} R_N} \tag{B-10}$$

$$R_{1,N} = R_{1,N-1} + \frac{T_{1,N-1}^2 R_N}{1 - R_{N-1,1} R_N} \tag{B-11}$$

Appendix C

MULTILAYER UNIAXIALLY ANISOTROPIC FLAT PANEL EQUATIONS

Using Figure 5 for a plane wave incident on a multilayer sheet of uniaxially anisotropic material, we have

$$r_i = \frac{\sqrt{\varepsilon_{iz} - \sin^2\theta} - \cos\theta\sqrt{\varepsilon_{ix}\varepsilon_{iz}}}{\sqrt{\varepsilon_{iz} - \sin^2\theta} + \cos\theta\sqrt{\varepsilon_{ix}\varepsilon_{iz}}} \qquad \text{parallel} \qquad \text{(C-1)}$$

$$= \frac{\cos\theta - \sqrt{\varepsilon_{ix} - \sin^2\theta}}{\cos\theta + \sqrt{\varepsilon_{ix} - \sin^2\theta}} \qquad \text{perpendicular} \qquad \text{(C-2)}$$

$$i = 1,2,\ldots N$$

These single-surface reflection coefficients in turn form the reflection and transmission coefficients for a single layer. They are

$$T_i = \frac{(1 - r_i^2)e^{-jk_i d_i}}{1 - r_i^2 e^{-j2k_i d_i}} \qquad \text{(C-3)}$$

$$R_i = \frac{r_i(1 - e^{-j2k_i d_i})}{1 - r_i^2 e^{-j2k_i d_i}} \qquad \text{(C-4)}$$

where

$$k_i = k_o\sqrt{\varepsilon_{ixz}(\varepsilon_{iz} - \sin^2\theta)} \qquad \text{parallel} \qquad \text{(C-5)}$$

$$k_o\sqrt{\varepsilon_{ix} - \sin^2\theta} \qquad \text{perpendicular} \qquad \text{(C-6)}$$

$$i = 1,2,\ldots N$$

with $k_o = 2\pi/\lambda_o$ and $\varepsilon_{ixz} = \varepsilon_{ix}/\varepsilon_{iz}$. R_i and T_i can then be used to form the overall reflection and transmission coefficients for many layers as in Appendix B.

Appendix D

VON KARMAN GEOMETRY

In two dimensions, the Von Karman equation is

$$y = \frac{D}{2\sqrt{\pi}} \left\{\cos^{-1}\left(1 - \frac{2(x+h)}{\ell}\right) - \frac{1}{2}\sin\left[2\cos^{-1}\left(1 - \frac{2(x+h)}{\ell}\right)\right]\right\}^{1/2} \quad \text{(D-1)}$$

where D is the diameter, ℓ is the length, and h is the antenna gimbal position. The first derivative or slope is

$$\frac{dy}{dx} = \frac{D}{4\sqrt{\pi}\sqrt{x+h}\sqrt{\ell-h-x}} \left\{1 - \cos\left[2\cos^{-1}\left(1 - \frac{2(x+h)}{\ell}\right)\right]\right\}$$

$$\times \left\{\cos^{-1}\left(1 - \frac{2(x+h)}{\ell}\right) - \frac{1}{2}\sin\left[2\cos^{-1}\left(1 - \frac{2(x+h)}{\ell}\right)\right]\right\}^{-1/2} \quad \text{(D-2)}$$

The second derivative is given by

$$\frac{d^2y}{dx^2} = \frac{D}{4\sqrt{\pi}} t^2 v\left[\left(-tu(\ell - 2(x+h)\right) + 4s - u^2v^2\right] \quad \text{(D-3)}$$

where

$$t = \left\{(x+h)[\ell - (x+h)]\right\}^{-1/2}$$

$$v = \left\{\cos^{-1}\left(1 - \frac{2(x+h)}{\ell}\right) - \frac{1}{2}\sin\left[2\cos^{-1}\left(1 - \frac{2(x+h)}{\ell}\right)\right]\right\}^{-1/2}$$

$$u = 1 - \cos\left[2\cos^{-1}\left(1 - \frac{2(x+h)}{\ell}\right)\right]$$

$$s = \sin\left[2\cos^{-1}\left(1 - \frac{2(x+h)}{\ell}\right)\right]$$

and the curvature at any point on the Von Karman curve (Equation D-1) is

$$K = \frac{\left|\frac{d^2y}{dx^2}\right|}{\left[1 + \left(\frac{dy}{dx}\right)^2\right]^{3/2}} \qquad \text{(D-4)}$$

The radius of curvature at any point is given by

$$R = \frac{1}{K} \qquad \text{(D-5)}$$

INITIAL DISTRIBUTION

1 Naval Air Systems Command (AIR-7220)
2 Naval Sea Systems Command (SEA-09B312)
1 Commander in Chief, U.S. Pacific Fleet (Code 325)
1 Commander, Third Fleet, Pearl Harbor
1 Commander, Seventh Fleet, San Francisco
2 Naval Academy, Annapolis (Director of Research)
2 Naval Ship Weapon Systems Engineering Station, Port Hueneme
    Code 5711, Repository (2)
    Code 5712 (1)
1 Naval Surface Weapons Center, White Oak Laboratory, Silver Spring, MD (W. T. Mesick)
1 Naval War College, Newport
1 Air Force Intelligence Service, Bolling Air Force Base (AFIS/INTAW, Maj. R. Lecklider)
1 Army Missile Command, Redstone Arsenal (K. Lebon)
1 Air Force Wright Aeronautical Laboratories, Wright-Patterson Air Force Base (AFWAL/AADM, A. E. Blume)
1 Air Force Wright Aeronautical Laboratories, Wright-Patterson Air Force Base (AFWAL/MLPO, D. Evans)
12 Defense Technical Information Center
1 Acurex Corporation, Huntsville, AL (F. A. Strobel)
1 Flight Systems, Inc., Newport Beach, CA (B. J. Crowe)
1 General Dynamics Corporation, Electronics Division, San Diego, CA (Dr. G. Tricoles)
1 Georgia Institute of Technology, Atlanta, GA (Dr. E. Joy, Department of Electrical Engineering)
1 Lockheed Aircraft Service Co., Ontario, CA (D. Hudson, Department 1333)
2 Martin-Marietta Aerospace, Orlando, FL
    G. K. Huddleston, MP 200 (1)
    E. A. Welsh, MP 450 (1)
1 Rogers Corporation, Lithonia, GA (S. Keahey)
2 Texas Instruments, Inc., Dallas, TX
    MS 333
        K. Hollenbeck (1)
        D. L. Purinton (1)
1 The Boeing Company, Seattle, WA (J. Schorgh, MS 47-36)
1 The Johns Hopkins University, Applied Physics Laboratory, Laurel, MD (L. B. Weckesser)

Best Available Copy